고유진동수 이용 손상추정법과 모드형상 이용 손상추정법에 의한 PSC 보의 비파괴 손상검색

Nondestructive Damage Detection in PSC Beams: Frequency-Based Method Versus Mode-Shape-Based Method

김 정 태† 류 연 선* 조 현 만**
Kim, Jeong-Tae Ryu, Yeon-Sun Cho, Hyun-Man
(논문접수일 : 2001년 3월 14일 ; 심사종료일 : 2001년 12월 12일)

요 지

PSC 보의 비파괴 손상검색을 위한 고유진동수 이용 손상추정법과 모드형상 이용 손상추정법을 제시하였다. 먼저, 고유진동수의 변화를 사용하여 손상의 위치를 예측하는 알고리즘과 고유진동수 1차 섭동 이론에 근거하여 균열크기를 예측하는 알고리즘을 요약하였다. 다음으로, 모드형상의 변화로부터 모드민감도의 변화를 감지하고 이를 통해 손상의 위치와 크기를 추정하는 손상지수 알고리즘을 요약하였다. PSC 보의 유한요소모델을 사용하는 수치실험을 통해 고유진동수 이용 손상추정법과 모드형상 이용 손상추정법의 정확성을 검증하였다. 분석결과 두 방법 모두 실험 대상 구조에 도입된 균열의 위치를 정확하게 예측 하였으며 균열의 크기를 비교적 근사하게 예측하였다.

핵심용어 : 구조식별, 손상검색, 고유진동수, 모드형상, PSC 구조, 구조안전도

Abstract

A methodology to nondestructively locate and estimate size of damage in beam-type structures using a few natural frequencies or a few mode shapes is presented. A damage-localization algorithm to locate damage from changes in natural frequencies and a damage-sizing algorithm to estimate crack-size from natural frequency perturbation are outlined. A damage index algorithm to localize and estimate severity of damage from monitoring changes in mode shapes is outlined. The frequency-based method and the mode-shape-based method are evaluated for several damage scenarios by locating and sizing damage in PS concrete beams for which a few natural frequencies and mode shapes are generated from finite element models. The result of the analyses indicates that the two methods correctly localize and closely estimate the size of the crack simulated in the test beam.

Keywords : *Structural identification, damage detection, natural frequency, mode shape, PSC structure, structural safety*

† 책임저자, 정회원 · 부경대학교 해양공학과 부교수
전화: 051-620-6227; Fax: 051-628-8146
E-mail: idis@pknu.ac.kr
* 정회원 · 부경대학교 해양공학과 교수
** 정회원 · 부경대학교 해양공학과 시간강사

• 이 논문에 대한 토론을 2002년 6월 29일까지 본 학회에 보내주시면 2002년 9월호에 그 결과를 게재하겠습니다.

1. Introduction

During the past two decades, a significant amount of research has been conducted in the area of NDD via changes in the modal response of a structure. The NDD methods developed up to date can be classified into four levels[1]: (1) Level I Methods, i.e., those methods that only identify if damage has occurred[2),3)]; (2) Level II Methods, i.e., those methods that identify if damage has occurred and simultaneously determine the location of damage[4)~6)]; (3) Level III Methods, i.e., those methods that identify if damage has occurred, determine the location of damage as well as estimate the severity of damage[7)~10)]; and (4) Level IV Methods, i.e., those methods that identify if damage is occurred, determine the location of damage, estimate the severity of damage, and evaluate the impact of damage on the structure.

The most common modal features that are used in Levels II and III are natural frequencies and mode shapes. Many researchers have attempted to detect and localize damage using changes in natural frequencies.[4),10)~13)] The appealing feature is that the natural frequencies are relatively simple to measure from and apply for the further use to structures. However, the feasibility of using frequency changes for the purpose of damage localization is limited for at least two reasons and an improved algorithm is needed for the same reasons. First, significant damage may cause very small changes in natural frequencies, particularly for larger structures, and these changes may go undetected due to measurement or processing errors. Next, variations in structural mass or measurement temperature cause uncertainty in measured frequency changes that further hamper the effectiveness of using frequency changes for damage localization. In an effort to overcome these difficulties, research efforts have focused on using changes in mode shapes.[14)~18)] The appealing feature is that the mode shapes are much more sensitive to damage than natural frequencies. However, the feasibility of using mode shapes is also challenged by many reasons. First, damage is typically local phenomenon and may not significantly influence mode shapes of the lower modes that are usually measured from vibration tests of large structures. Second, mode shapes are often exposed to random noises that may be induced from various sources such as ambient signals or inconsistent sensor positions that set before and after damage. Third, the number of sensors and the choice of sensor coordinates have crucial effects on the accuracy of damage detection practice. Among these several problems, we bring this study into focus on the development of improved damage detection algorithms that utilize limited modal parameters(e.g., a few frequencies or a few mode shapes).

In this paper we present a nondestructive damage detection methodology to locate and estimate size of damage in beam-type structures for which a few natural frequencies or a few mode shapes are available. First, a frequency-based damage detection(FBDD) method is outlined. A damage-localization algorithm to locate damage from changes in natural frequencies and a damage-sizing algorithm to estimate crack-size from natural frequency perturbation are formulated. Next, a mode-shape-based damage detection(MBDD) method is outlined. A damage index algorithm to localize and estimate severity of damage from monitoring changes in modal strain energy is formulated. Finally, the FBDD method and the MBDD method are evaluated for several damage scenarios by locating and sizing damage in PS concrete beams for which a few natural frequencies and mode shapes are generated from finite element models.

2. Theory of Nondestructive Damage Detection

The NDD methodology presented here is designed to yield information on location and severity of damage directly from changes in modal characteristics of the target structure. The modal characteristics of interest here are natural frequencies and mode shapes. Once two sets of modal parameters are measured for the as-built structure and its corresponding damaged state, the NDD to be described here is used to predict damage location and to estimate the severity of the damage at that location of the structure.

2.1 FBDD Method

(1) Damage-Localization Algorithm[19]

With reference to Fig. 1, suppose we are given an undisturbed(i.e., undamaged) *MDOF* structural system that yields the ith natural frequency ω_i and ith mode shape ϕ_i. Next, assume that at some later time the structure is damaged(e.g., as shown in Fig. 1) in one or more locations of the structure. The resulting characteristic equation of the damaged structure yields ω_i^* and ϕ_i^*. Note that the asterisk denotes the damaged state.

For the *MDOF* structural system of *NE* elements and N nodes, the damage inflicted at predefined locations may be predicted using the following sensitivity equation[7]:

$$\sum_{j=1}^{NE} F_{ij}\alpha_j = Z_i \tag{1}$$

in which $\alpha_j(-1 \le \alpha_j \le 0)$ is the damage inflicted at the jth location, i.e., the fractional reduction in jth element's stiffness parameter. By neglecting changes in mass, the term Z_i that is the fractional change in the ith eigenvalue due to damage is given by:

$$Z_i = \theta\omega_i^2/\omega_i^2 \tag{2}$$

where $\delta\omega_i^2 = \omega_i^{*2} - \omega_i^2$. The term F_{ij} is the fraction of modal energy(i.e., sensitivity) for the ith mode that is concentrated in jth element and is given by:

$$F_{ij} = \frac{\{\phi_i\}^T[C_j]\{\phi_i\}}{\{\phi_i\}^T[C]\{\phi_i\}} \tag{3}$$

where $\{\phi_i\}$ is the ith mode shape vector, $[C]$ is the system stiffness matrix, and $[C_j]$ is the contribution of the jth element to the system stiffness.

Once the quantity Z_i is experimentally determined and the sensitivity F_{ij} is numerically generated, Eq. (1) can be solved to locate and size damage in the system. However, the inverse solution is possible only if the number of damage parameters is close to the number of modes (i.e., $NE \approx NM$).[16] In the case when $NE \gg NM$, the system becomes illconditioned and alternate methods to estimate damage parameters should be sought. In an effort to overcome this difficulty, we formulate an algorithm using frequency-change ratio and sensitivity ratio that are based on earlier works presented by Stubbs et al.[10] and Cawley and Adams.[4]

Let us consider the structural system of *NE* elements ($j = 1, 2, \cdots, q, \cdots, NE$) and a measured set of *NM* vibrational modes ($i = 1, \cdots, m, n, \cdots, , NM$). Equation (1) is rewritten for any two modes m and n ($m \neq n$), respectively. On dividing Eq. (1) for mode m by another Eq. (1) for mode n, we obtain by:

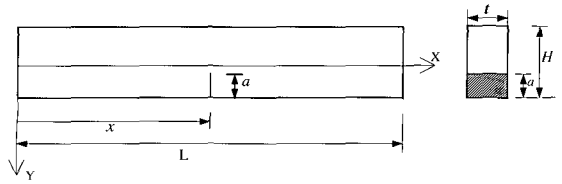

Fig. 1 Geometry of Beam with a Crack

$$\frac{Z_m}{Z_n}=\frac{\sum_{j=1}^{NE}F_{mj}\alpha_j}{\sum_{j=1}^{NE}F_{nj}\alpha_j} \tag{4}$$

$$=\frac{F_{m1}\alpha_1+F_{m2}\alpha_2+\cdots+F_{mq}\alpha_q+\cdots+F_{mNE}\alpha_{NE}}{F_{n1}\alpha_1+F_{n2}\alpha_2+\cdots+F_{nq}\alpha_q+\cdots+F_{nNE}\alpha_{NE}}$$

Assuming that the structure is damaged in a single element q, such that $\alpha_j \neq 0$ when $j=q$ but $\alpha_j=0$ when $j\neq q$, Eq. (4) is rewritten by:

$$Z_m/Z_n=F_{mq}/F_{nq} \tag{5}$$

in which Z_m/Z_n is the ratio of the fractional change in mth eigenvalue to the fractional change in nth eigenvalue. Also, F_{mq}/F_{nq} is the ratio of the sensitivity for mth mode and qth element to the sensitivity of nth mode and qth element. So the damage inflicted at that location is defined using Eq. (5) when the L.H.S equals to the R.H.S.

For all measured NM modes, Eq. (5) can be extended into:

$$Z_m\Big|\sum_{k=1}^{NM}Z_k=F_{mq}\Big|\sum_{k=1}^{NM}F_{kq} \tag{6}$$

Since Eq. (6) is true only if element q is damaged, we introduce an error index into Eq. (6) as follows:

$$e_{ij}=Z_i\Big|\sum_{k=1}^{NM}Z_k-F_{ij}\Big|\sum_{k=1}^{NM}F_{kj} \tag{7}$$

where e_{ij} represents localization error for the ith mode and the jth location, and $e_{ij=0}$ indicates that the damage is located at the jth location using the ith modal information. To account for all available modes we form a single damage indicator(DI) for the jth member as:

$$DI_j=\left[\sum_{i=1}^{NM}e_{ij}^2\right]^{-1/2} \tag{8}$$

where $0\leq DI_j<\infty$ and the damage is located at element j if DI_j approaches the local maximum point.

(2) Damage-Sizing Algorithm[19]

Assuming no volume changes due to cracks or other geometrical changes, Gudmunson[20] proposed a first order perturbation method that predicts the changes in natural frequencies of a structure resulting from the damage. According to Gudmunson,[20] for small cracks, the fractional changes in modal strain energy can be related to the fractional changes in frequency as follows:

$$\frac{\delta W_i}{W_i}=\frac{\delta\omega_i^2}{\omega_i^2} \tag{9}$$

where W_i is the ith modal strain energy of the initial structure, δW_i is the loss in the ith modal strain energy after damage, and $\delta\omega_i^2/\omega_i^2$ is the fractional change in the ith eigenvalue due to the damage.

In the present study, we limit our discussion on the crack-size model to Euler-Bernoulli beams. If the Euler-Bernoulli beam theory is used, the ith modal strain energy W_i is given by:

$$W_i=\int_0^L\frac{1}{2}EI\{\phi_i''(x)\}^2dx \tag{10}$$

where E is Young's modulus, I is the second moment of area, L is the beam span length, and $\phi_i(x)$ is the ith mode shape function. Next, the change in the ith modal strain energy due to the crack(e.g., as shown in Fig. 1) can be computed by implementing linear elastic fracture mechanics. On assigning plane strain condition to the cracked beam, the energy loss rate of the ith modal strain energy is given by:

$$\frac{\partial\delta W_i}{\partial a}=t\frac{(1-\nu^2)}{E}K_I^2 \tag{11}$$

where $\partial\delta W_i/\partial a$ is the energy loss rate of the ith modal strain energy W_i with respect to crack depth a; t is the beam thickness; ν is Poisson's ratio; and K_I is the stress intensity factor depending on crack depth a, applied flexural stress level σ, and beam dimension (e.g., thickness t, height H and length L).

For the edge-crack case under bending motion (e.g., as shown in Fig. 1), the stress intensity factor is given by:

$$K_I = F \cdot \sigma\sqrt{\pi a} \tag{12}$$

The term F is a geometrical factor depending on dimensionless crack depth ratio a/H and $F=1.12$ for small cracks. Substituting Eqs. (12) into Eq. (11) and further integrating Eq. (11) over the crack contour generates:

$$\delta W_i = \left(\frac{\pi t(1-\nu^2)}{2E} F^2 \sigma_k^2 a_k^2 \right)_i \tag{13}$$

in which, for the ith mode, $a_k = a(x_k)$ represents the crack size at location x_k and $\sigma_k = \sigma(x_k)$ represents the maximum flexural stress at location x_k along the beam's longitudinal axis. For the Euler-Bernoulli beam, the stress level is given by

$$\sigma(x_k) \frac{1}{2} EH\phi_i''(x_k) \tag{14}$$

On dividing Eq. (13) by Eq. (10), the fractional change in the ith modal strain energy is given by

$$\frac{\delta W_i}{W_i} = \frac{\pi t(1-\nu^2)}{4} \frac{H^2}{I} F^2 S_{ik} a_k^2 \tag{15}$$

in which S_{ik} represents the sensitivity of the ith modal strain energy at the kth location and is given by:

$$S_{ik} = \int_k \{\phi_i''\}^2 dx \Big/ \int_0^L \{\phi_i''\}^2 dx \tag{16}$$

On substituting Eq. (10) - Eq. (15) into Eq. (9), we obtain a relationship between the crack depth and the fractional changes in the ith eigenvalue as follows:

$$\frac{\delta\omega_i^2}{\omega_i^2} = \eta S_{ik} \left(\frac{a_k}{H} \right)_i^2 \tag{17}$$

and for the beam section considered here:

$$\eta = 0.25\pi t(1-\nu^2) F^2 H^4 I^{-1} \tag{18}$$

in which $(a_k/H)_i$ is the dimensionless crack size at the kth location defined in the ith mode and η is a constant value depending on beam dimensions, crack types, and Poisson's ratio. Equation (17) can be solved to estimate crack sizes if the quantities $\delta\omega_i^2/\omega_i^2$ and S_{ik} are experimentally determined or numerically generated.

2.2 MBDD Method[18]

Consider a homogeneous, uniform cross-sectional, one-dimensional beam with NE elements(in the finite element sense) and N nodes. Assume that the input-output relationship of the beam is linear. Assuming a solution of the associated dynamic eigenvalue problem, the ith modal stiffness, K_i, of the beam is given by:

$$K_i = \int_0^L k(x)[\phi_i''(x)]^2 dx \tag{19}$$

where $\phi_i(x)$ is the mode shape of ith modal vector and $k(x)$ is the bending stiffness of the beam(i.e., the product of Young's modulus and the second moment of area). The contribution of the jth element to the ith modal stiffness, K_{ij}, is given by:

$$K_{ij} = k_j \int_j [\phi_i''(x)]^2 dx \tag{20}$$

where k_j is the stiffness of the jth element and the integral is over the jth element.

The fraction of the modal energy for the ith mode that is concentrated in jth member(i.e., sensitivity of the ith modal stiffness with respect to jth element) is given by[21]:

$$F_{ij} = K_{ij} / K_i \tag{21}$$

Let the corresponding modal parameters in Eqs. (19)-(21) associated with the damaged structure be characterized by asterisks. Then for the damaged structure

$$F_{ij}^* = K_{ij}^* / K_i^* = F_{ij} + \delta F_{ij} \tag{22}$$

where scalars K_{ij}^* and K_i^* are given by:

$$K_{ij}^* = k_j^* \int_j [\phi_i''^*(x)]^2 dx \tag{23}$$

and

$$K_i^* = k_j^* \int_0^L k^*(x) [\phi_i''^*(x)]^2 dx \tag{24}$$

The term δF_{ij} represents the variation of the fraction of modal energy at the jth member and for the ith mode. On differentiating Eq. (22), the quantity δF_{ij} is given by:

$$\delta F_{ij} = \frac{K_{ij}}{K_i} \left[\frac{\delta K_{ij}}{K_{ij}} - \frac{\delta K_i}{K_i} \right] \tag{25}$$

Assuming $K_i \gg K_{ij}$ (when $\gg 1$), Eq. (25) can be further simplified:

$$\delta F_{ij} \cong \frac{\delta K_{ij}}{K_i} \tag{26}$$

Thus the quantity δF_{ij} in Eq. (26) can be measured directly from changes in modal parameters.

Assuming the structure is damaged in ND multiple locations, $\delta K_{ij} \approx \delta K_i / ND$. The quatient $\delta K_{ij} / K_i$ can be approximated by the fractional change in the ith eigenvalue due to damage by[7]:

$$g_i \frac{\delta K_{ij}}{K_i} \approx \frac{1}{ND} \left(\frac{\delta \omega_i^2}{\omega_i^2} \right) \tag{27}$$

in which g_i is a dimensionless factor representing the fractional change in the ith modal parameters. The term δK_{ij} represents the variation of the modal stiffness and from Eqs. (20)-(24), it is given by:

$$\delta K_{ij} = K_{ij}^* - K_{ij} = \gamma_{ij}^* k_j^* - \gamma_{ij} k_j \tag{28}$$

where $\gamma_{ij} = \int_j [\phi_i''(x)]^2 dx$ and $\gamma_{ij}^* = \int_j [\phi_i''(x)]^2 dx$. Next, by assuming that Young's modulus and the second moment of area are constant over the entire beam (i.e., $k(x) = k(\hat{x})$ for $0 \le x \le L$), and further on approximating the stress distribution in Eq. (19) by $k_j = k(\hat{x})$ for $j = 1, NE$), the right-hand side of Eq. (26) can be rewritten as:

$$\frac{\delta K_{ij}}{K_i} = \frac{k_j^* \gamma_{ij}^* - k_j \gamma_{ij}}{k_j \gamma_i} \tag{29}$$

where $\gamma_i = \int_0^L [\phi_i''(x)]^2 dx$.

On equating Eq. (27) into Eq. (29), the relative change in jth element stiffness is given by

$$\frac{k_j}{k_j^*} = \frac{\gamma_{ij}^*}{\gamma_i g_i + \gamma_{ij}} \tag{30}$$

Equation (30) is extended into all measured NM modes. To account for several measurable and identifiable modes, the damage localization

index for the jth location, β_j, is given by:

$$\beta_j = \frac{k_j}{k_j^*} = \sum_i \gamma_{ij}^* / \sum_i (\gamma_i g_i + \gamma_{ij}) \quad (31)$$

where damage is indicated as the relative change in jth element stiffness when the *L.H.S.* of Eq. (31) is greater than one.

Once damage is located at the jth element, the severity of damage is estimated at the same element directly from Eqs. (30) and (31). The severity estimation index for jth location, α_j, is given by:

$$\alpha_j = \frac{k_j^* - k_j}{k_j} = \left(\sum_i (\gamma_{ij} - \gamma_{ij}^*) + \sum_i \gamma_i g_i\right) / \sum_i \gamma_{ij}^* \quad (32)$$

where the damage severity is the fractional change in stiffness of the jth element.

3. Numerical Experiment

3.1 Description of Test Structure

A numerical experiment was performed to evaluate the proposed FBDD and MBDD methods. A simply supported PS concrete beam was selected (see[6] for detailed explanation on the target structure) and modal responses of the structure were generated using finite element models before and after damaging episodes. As shown in Fig. 2, the test structure was the FE model of the PS concrete beam with the length L=3.6-m and the rectangular cross-section $t \times H$=0.1-m×0.125-m. For modal analysis purposes we divided the beam into 28,512 block elements. The steel tendon is placed to center by 288 elements along the beam and each element size is 1cm×1.25cm ×1.25cm. All others are concrete elements and each element size is 1.125cm×1.125cm×1.25cm. Material properties of the FE model were assigned

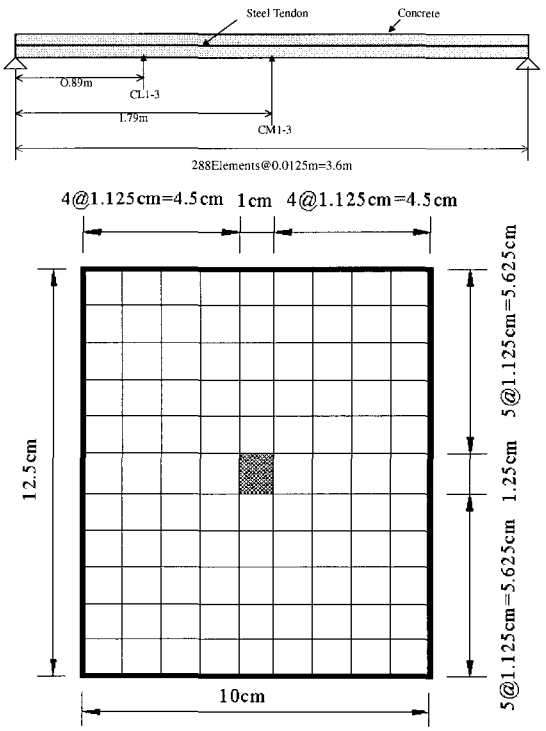

Fig. 2 Schematic of Test Structure

as follows: (1) for concrete elements, the elastic modulus E=25GPa, Poisson's ratio ν=0.18, and the linear mass density ρ=2300kg/m^3; and (2) for steel tendon elements, 210GPa, Poisson's ratio ν=0.3, and the linear mass density ρ= 7850kg/cm^3.

The pre-damage and post-damage modal parameters of the FE model were generated numerically using the commercial software ANSYS. Here, six damage cases were investigated as summarized in Table 1. As shown in Fig. 2 and Fig. 3, damage was simulated by a designed crack-depth for each damage case and was inflicted by eliminating the stiffness of the appropriate elements in the FE model. Note that the thickness of the crack was defined as the length of an element (i.e., 1.25-cm). The first three damage cases CL1~CL3(listed Table 1) were simulated by the cracks inflicted at 0.89m location(e.g., x/L

Table 1 Damage Scenarios and Natural Frequencies of Test Beam

Damage Case	Inflicted Damage			Natural Frequency (Hz)	
	Location (x/L)	Crack-size (a/H)	Severity ($\Delta EI/EI$)	Mode 1	Mode 2
Reference	-	-	-	11.196	44.074
CL1	0.248	0.09	-0.24	11.162	43.857
CL2	0.248	0.27	-0.59	11.019	42.701
CL3	0.248	0.45	-0.78	10.746	40.825
CM1	0.498	0.09	-0.24	11.142	44.074
CM2	0.498	0.27	-0.59	10.849	44.072
CM3	0.498	0.45	-0.78	10.350	44.064

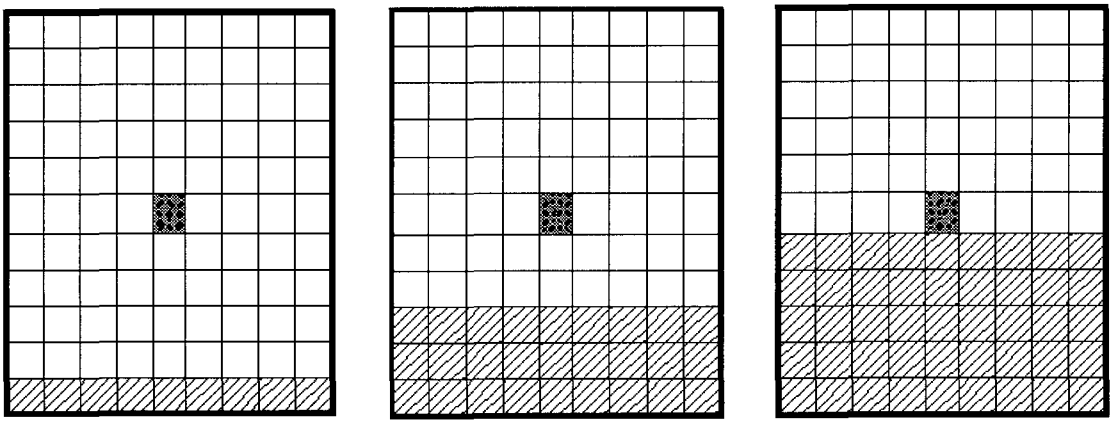

(a) a/H=0.09 (b) a/H=0.27 (c) a/H=0.45

Fig. 3 Damage Simulation to the Test Structure

=0.248) from the left edge which is the vicinity of the left quarter-span. The remaining three damage cases CM1~CM3(listed in Table 1) were simulated by the cracks inflicted at 1.79m location(e.g., x/L=0.498) which is the vicinity of the mid-span.

The extracted modal parameters of the test structure included the pre-damage and post-damage frequencies and mode shapes of the first two bending modes. The natural frequencies for the undamaged state and the six damage cases are listed in Table 1. The mode shape vectors were read at 11 locations that are equally spaced along the top centerline of the beam's longitudinal axis(e.g., 36cm between two adjacent locations). The undamaged mode shapes of the test structure are shown in Fig. 4. Also, the undamaged mode shapes were compared to the post-damage mode shapes as shown in

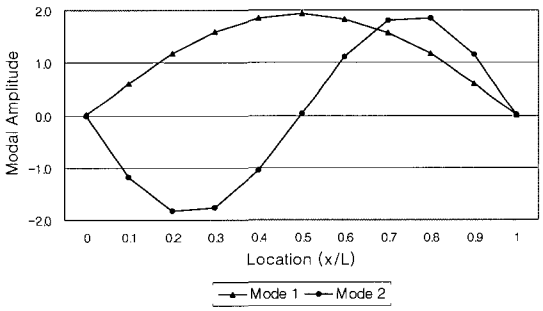

Fig. 4 Pre-Damage Mode Shapes of Test Structure

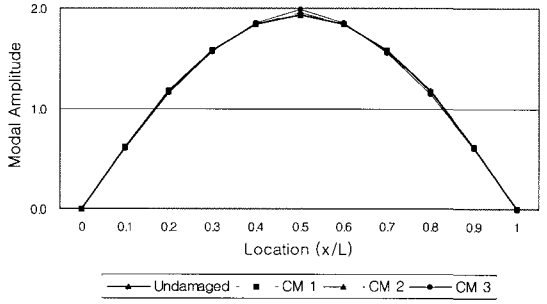

(a) Mode 1

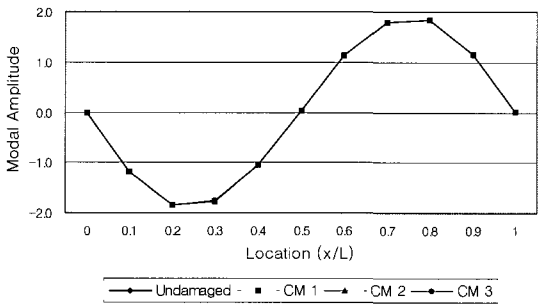

(b) Mode 2

Fig. 5 Comparison of 1st Mode Shapes : Undamaged Vs Damage Cases CM1-CM3

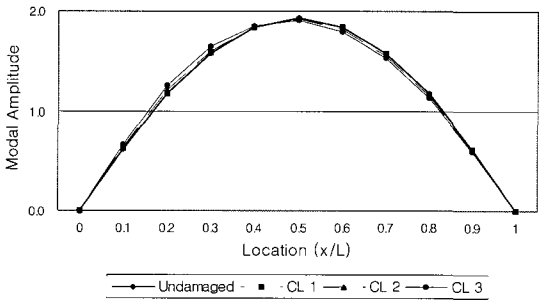

(a) Mode 1

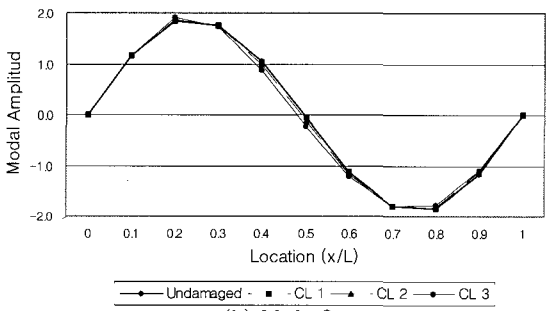

(b) Mode 2

Fig. 6 Comparison of 2nd Mode Shapes : Undamaged Vs Damage Cases CL1-CL3

Figs. 5 and 6. Figure 5 shows the mode shapes of the modes 1 and 2 obtained before and after the cracks were inflicted at the left quarter-span(i.e., CL1~CL3). Figure 6 shows the mode shapes of the modes 1 and 2 obtained before and after the cracks were inflicted at the mid-span(i.e., CM1~CM3). Note from the Figures that bare amplitude changes in the mode shapes are not sensitive enough to monitor and localize damage at the inflicted locations.

3.2 Damage Detection by FBDD Method

The Euler-Bernoulli beam model was selected as the damage detection model(DDM), i.e., the mathematical representation for damage detection practice. Modal parameters needed for the FBDD process are pre-damage and post-damage natural frequencies and pre-damage mode shapes. The DDM of the structure consists of total 288

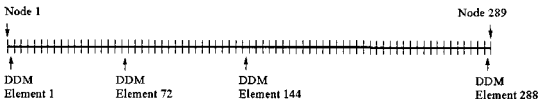

Fig. 7 Schematic of Damage Detection Model

beam elements of equal size, as schematized in Fig. 7(note that the DDM elements 1~288). Each DDM element is a potential damage location and has a spacing of 1.25-cm or 0.347 percent (i.e., 1/288×100) of the beam span. We justify the use of a 1.25-cm wide element by interpolating measured modal vectors at the 289 nodal points of the damage detection model obtained by the use of spline functions and the element modal amplitude values from the mode shapes(i.e., Fig. 4) of the FE model. Using the interpolated modal coordinates for the beam, we generated functions $\phi(x)$, where x is the coordinate along the axis of the beam.

The modal sensitivity(i.e., the equivalent ex-

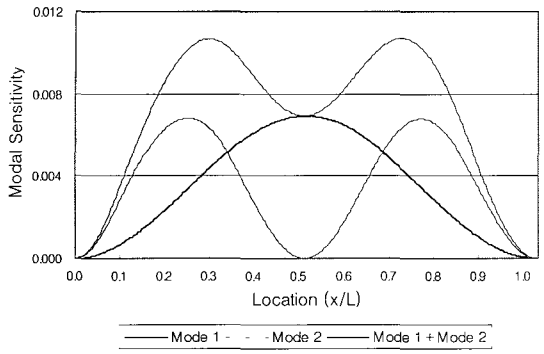

Fig. 8 Modal Sensitivities of Test Structure

pression of Eq. (3)) of mode i and element j between two locations (x_j, x_{j+1}) was computed by[21]:

$$F_{ij}=\int_{x_j}^{x_{j+1}} EI\{\phi_i''(x)\}^2\frac{dx}{K_i}\ ;$$
$$K_i=\int_0^l EI\{\phi_i''(x)\}^2dx \qquad (33)$$

The curvatures $\phi''(x)$ of the mode shapes were generated at the 289 nodes of the damage detection model. Since two natural frequencies are available, the sensitivities are defined for 2 modes and 288 DDM elements. Fig. 8 shows the modal sensitivities of the test beam that were computed along the beam's longitudinal axis. It is observed that either the individual modal sensitivities or the combined sensitivities are indicative for most locations throughout the span except for the both ends of the simply supported beam. The maximum sensitivity of the 1st mode is at the mid-span and that of the 2nd mode at the quarter-span. Note that the single second mode is not sensitive to locations near the mid-span.

The fractional changes in frequencies(i.e., Eq. (2)) were computed by using the frequency results listed in Table 1. By assuming that the flexural rigidity EI is constant over the beam span, the sensitivity ratio(i.e., the right-hand side of Eq. (17)) for an element q and for any two modes m and n can be rewritten by:

$$\frac{F_{mq}}{F_{nq}}=\frac{\int_q\{\phi_m''\}^2dx}{\int_q\{\phi_n''\}^2dx}\cdot\frac{\int_q^l\{\phi_n''(x)\}^2dx}{\int_q^l\{\phi_m''(x)\}^2dx} \qquad (34)$$

Next, we computed localization errors using Eq. (7) for 2 modes and 288 locations(i.e., e_{1j} and e_{2j}, $j=1,288$) by implementing the sensitivity ratios and the fractional changes in frequencies. Error indices for the damage cases CM1~CM3 are plotted in Fig. 9 and error indices for CL1~CL3 are plotted in Fig. 10. In the Figures, note that each point where error equals to zero indicates that a crack is located at that location. Finally, we computed the single damage index given by Eq. (8) to decide potential crack locations.

For example, damage indices of damage cases CL2 and CM2 are plotted in Figs. 11 and 12.

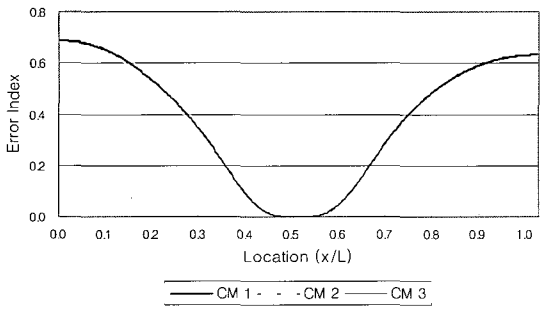

Fig. 9 Error Indices for Damage Cases CM1-CM3

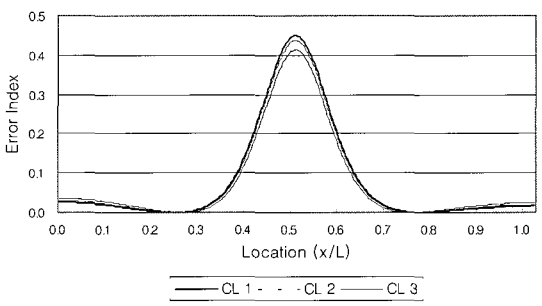

Fig. 10 Error Indices for Damage Cases CL1-CL3

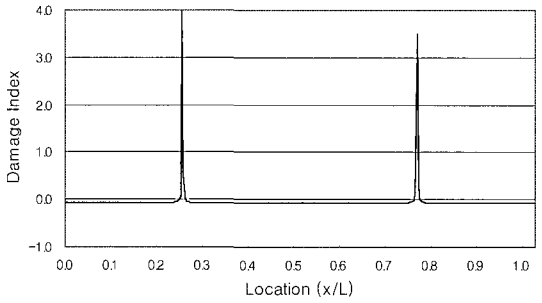

Fig. 11 Damage Localization Results of FBDD Method : Damage Case CL2

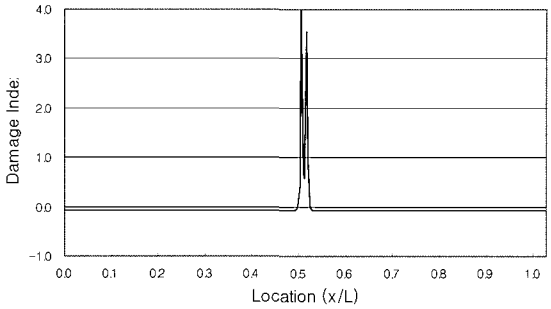

Fig. 12 Damage Localization Results of FBDD Method : Damage Case CM2

Table 2 Damage Prediction Results of Test Beam using FBDD Method

Damage Case	Inflicted Damage			Predicted Damage		
	DDM Element	Location(x/L)	Crack-size(a/H)	DDM Elements	Location(s)(x/L)	Crack-depth(a/H)
CL1	72	0.248	0.09	69, 219	0.238, 0.759	0.141, N/A
CL2	72	0.248	0.27	66, 217	0.227, 0.752	0.358, N/A
CL3	72	0.248	0.45	61, 213	0.210, 0.738	0.574, N/A
CM1	144	0.498	0.09	143, 144	0.495, 0.498	0.110, 0.110
CM2	144	0.498	0.27	142, 145	0.491, 0.502	0.276, 0.276
CM3	144	0.498	0.45	141	0.488	0.420, 0.420

respectively. In the Figures, two symmetric locations are predicted due to the symmetric motion of the modal strain energy(as described in Eq. (7)) for the simply supported beam. Thus one location is false-alarmed for each damage case. The damage localization results for the six damage cases are summarized in Table 2. Note that the prediction was made by either indicating DDM elements or dimensionless locations. In Fig. 11 the crack was simulated at the quarter-span and it is identical to the DDM element 72. The predicted peak was close to the simulated element. Also, in Fig. 12 the crack was simulated at the mid-span and the location is identical to the DDM element 144. The predicted peak was close to the simulated element.

The accuracy of the damage localization presented here is evaluated by measuring the so-called localization error $\leq = (\Delta x/L) \times 100$, in which Δx is the metrical difference between real crack location and predicted location and L is the reference span. From the comparison, it is observed that the minimum localization error is 0.3 percent(damage case CM1) and the maximum localization error is 3.8 percent(damage case CL3) by excluding the false-alarmed locations. It means that the predicted locations fall within 1-cm~13.7-cm of the correct locations in the test beam(note that 360-cm).

Damage size at each predicted location was estimated by using the damage-sizing model. Assuming a crack is located in element j between two locations (x_j, x_{j+1}), a solution of crack size is given by:

$$\left(\frac{a_k}{H}\right) = \sqrt{\frac{\delta\omega_i^2}{\eta \cdot S_{ik} \cdot \omega_i^2}} \tag{35}$$

where $(a_k/H)_i$ is the dimensionless crack size estimated at location x_k $(=(x_j+x_{j+1})/2)$ by using the ith modal data. The modal sensitivity of mode i and location k was computed using Eq. (33).

The constant η was obtained from Eq. (18) by implementing H=0.125m, L=3.6m, Poisson's ratio of 0.18, and the geometrical factor F=1.12. The fractional changes in the eigenvalues were computed from the pre-damage and post-damage frequencies listed in Table 1. The damage-sizing results for the six damage cases are summarized in Table 2.

The accuracy of the damage sizing is evaluated by measuring the size error, which represents the difference between real and predicted crack-depths. It is observed that for damage cases CL1-CL3 the size errors range 27.7 percent~56.6 percent and for CM1-CM3 the size errors range 2.2 percent~22 percent. For example, one-percent error means 0.1-mm difference in the estimation of 10-mm crack-depth.

3.3 Damage Detection by MBDD Method

The Euler-Bernoulli beam model was selected as the damage detection model for the MBDD method. As described previously(i.e., as shown in Fig. 7), the DDM of the structure consists of total 288 beam elements of equal size. Modal parameters needed in the MBDD process are pre-damage and post-damage mode shapes and frequencies. For individual mode shapes, pseudo readings at the 289 nodal points of the damage detection model were obtained via the use of spline functions. Using the interpolated modal coordinates for each mode shape, we generated functions $\phi(x)$ and $\phi''(x)$, where x is the coordinate along the axis of the beam. Then we computed the pre-damage and post-damage modal sensitivities, as shown in Figs. 13-16. Figures 13 and 14 show, respectively, the 1st and 2nd modal sensitivities of the test beam before and after the damage cases CL1-CL3. Figures 15 and 16 show, respectively, the 1st and 2nd modal sensitivities before and after the damage cases CM1-CM3. In these Figures note that changes in the mode sensitivities are indicative to the cracks inflicted at the left quarter-span(see Figs. 13 and 14) and also to the cracks inflicted at the mid-span (see Fig. 15).

Next, the damage localization index(i.e., Eq. (31)) of element j was computed for the six damage cases. Then the values of the indicator was normalized according to the rule:

$$Z_j=(\beta_j-\mu_{\beta j})/\sigma_{\beta j} \tag{36}$$

where $\mu_{\beta j}$ is the Mean of β_j and β_j is the standard deviation of β_j. The beam elements were next assigned to a damage class via a statistical-pattern-recognition technique that utilizes hypothesis testing. The null hypothesis(i.e., H_o) was taken to be the structure undamaged at the jth element and the alternate hypothesis(i.e., H_1) was taken to be the structure damaged at the jth element.

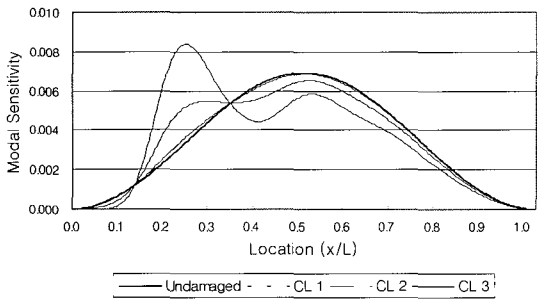

Fig. 13 Modal Sensitivity of 1st Mode: Predamage Vs Damage Cases CL1~CL3

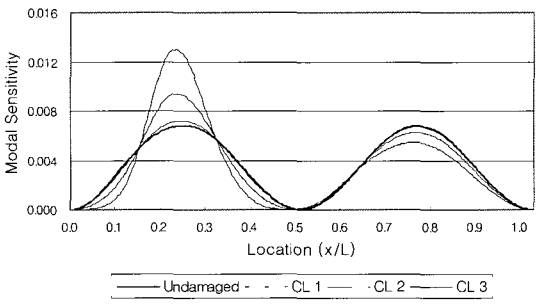

Fig. 14 Modal Sensitivity of 2nd Mode : Predamage Vs Damage Cases CL1~CL3

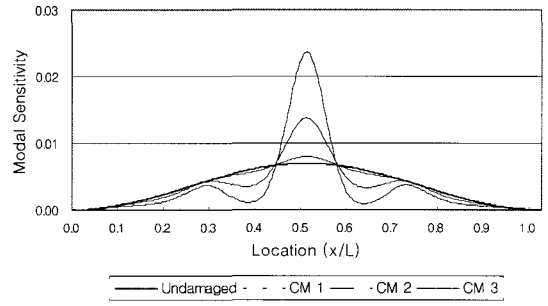

Fig. 15 Modal Sensitivity of 1st Mode : Predamage Vs Damage Cases CM1~CM3

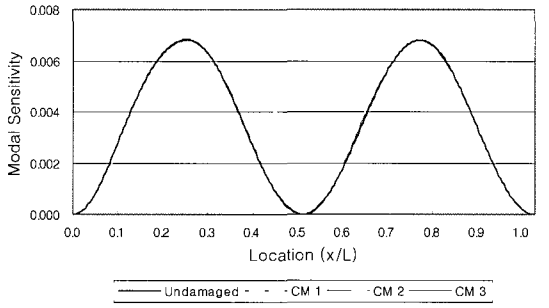

Fig. 16 Modal Sensitivity of 2nd Mode : Predamage Vs Damage Cases CM1~CM3

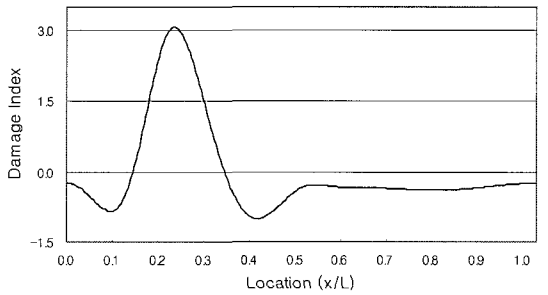

Fig. 17 Damage Localization Results of MBDD Method : Damage Case CL2

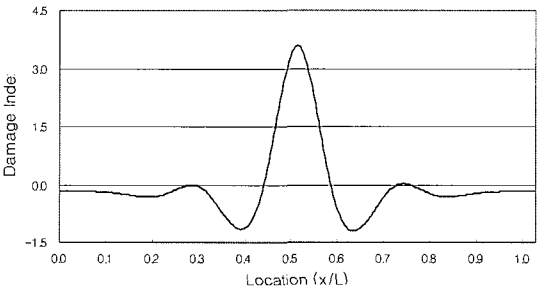

Fig. 18 Damage Localization Results of MBDD Method : Damage Case CM2

In assigning damage to a particular location, we utilized the following decision rule: (1) choose H_1 if $Z_j \geq 2$ and (2) choose H_o otherwise. This corresponds a test with the confidence level of 0.98.

The damage localization results for the six damage cases are listed in Table 3. For example, damage localization indices of damage cases CL2 and CM2 are plotted in Figs. 17 and 18, respectively. In the Figures the damage indices are greater than two in a region near to and including the peak locations. Note that in Fig. 17 the crack was simulated at the quarter-span and the location is the DDM element 72. The predicted peak element was close to the simulated element. Note also that in Fig. 18 the crack was simulated at the mid-span and the location is identical to the DDM element 144. The predicted peak element was identical to the simulated element. There is no damage in any other part of the structure. The accuracy of the damage localization is evaluated by measuring the localization error *le*. It is observed that the localization errors range 0 percent(CM1, CM2 and CM3)~1.54 percent(CL1,CL2, and CL3). The 1.54 percent error means that the predicted location deviates 6.25-cm from the correct location in the 3.6-m span length.

Once the damage was located, the severity estimation index(i.e., Eq. (32)) was computed for the predicted location. For each damage scenario, a damage-severity value was estimated at the peak locations listed in Table 3. The accuracy of the damage sizing is evaluated by measuring the size error that is the difference between inflicted and predicted severities of damage. It is observed that for damage cases CL1-CL3 the size errors range 34.7 percent~69.0 percent and for CM1-CM3 the size errors range 1.0 percent~45 percent.

Table 3 Damage Prediction Results of Test Beam using MBDD Method

Damage Case	Inflicted Damage			Predicted Damage		
	DDM Element	Location (x/L)	Severity ($\Delta EI/EI$)	Range of DDM Elements [Location]	Most Probable DDM Element [Location]	Severity ($\Delta EI/EI$)
CL1	72	0.248	-0.24	55~81 [0.191-0.280]	67 [0.233]	-0.074
CL2	72	0.248	-0.59	55~80 [0.191-0.277]	67 [0.233]	-0.364
CL3	72	0.248	-0.78	55~80 [0.191-0.277]	67 [0.233]	-0.509
CM1	144	0.498	-0.24	133~155 [0.48-0.52]	144 [0.498]	-0.132
CM2	144	0.498	-0.59	133~155 [0.48-0.52]	144 [0.498]	-0.538
CM3	144	0.498	-0.78	133~155 [0.48-0.52]	144 [0.498]	-0.788

4. Summary and Conclusions

This paper presented a methodology to non-destructively locate and estimate size of damage in structures for which a few frequencies or a few mode shapes are available. First, a frequency-based damage detection(FBDD) method was outlined. A damage-localization algorithm that locates damage from changes in natural frequencies and a damage-sizing algorithm that estimates crack-size from natural frequency perturbation were formulated. Next, a mode-shape-based damage detection(MBDD) method was outlined. A damage-index algorithm that locates and estimates severity of damage from changes in modal strain energy was formulated. The FBDD method and the MBDD method were evaluated for several damage scenarios by locating and sizing damage in PS concrete beams for which only a few modal parameters were available. For the verification test, natural frequencies and mode shapes of the first two bending modes were generated from finite element models.

By applying the FBDD approach to the test structure, it was observed that damage could be located with a relatively small localization error. The predicted locations fell within 1-cm (i.e., the cracks near the mid-span) and within 13.7-cm(i.e., the cracks near the left quarter-span) of the correct locations in the 3.6-m beam span. It was also observed that the size of crack could be estimated with a relatively small size error for the crack inflicted at the mid-span and a relatively large size error for the crack at the quarter-span. By applying the MBDD approach to the test structure, it was observed that damage could be located with the high accuracy. The predicted locations were identical to the inflicted locations(i.e., the cracks near the mid-span) and were within 6.25-cm from the correct locations(i.e., the cracks near the left quarter-span) in the 3.6-m beam span. It was also observed that the severity of the damage could be estimated with a relatively small size error for the cracks inflicted at the mid-span and a relatively large size error for the cracks at the quarter-span.

Research to improve the damage detection algorithms presented is continuing along two lines of inquires. First, we are extending to quantify the effect of uncertainty due to measurement or modeling errors on the accuracy of

damage identification. Second, we are extending the methodology to more complicated structures such as 3-D frames.

Acknowledgment

The authors wish to acknowledge the financial support of the Korea Research Foundation made in the program year 1999.

References

1. Rytter, A., "Vibration Based Inspection of Civil Engineering", Ph.D. Dissertation, University of Aalborg, Denmark, 1993
2. Vandiver, J. K., "Detection of Structural Failures on Fixed Platforms by Measurement of Dynamic Responses", Proc. of 7th Annual Offshore Technology Conference, Houston, Texas, Paper 2267, 1975
3. Crohas, H., and Lepert, P., "Damage Detection Monitoring Method for Offshore Platforms Is Field Tested", *Oil and Gas J.*, Vol. 80, No. 8, 1982
4. Cawley, P., and Adams, R. D., "The Location of Defects in Structures from Measurements of Natural Frequencies", *J. Strain Analysis*, Vol. 14, No. 2, 1979, pp.49~57
5. Pandey, A. K., Biswas, M., and Samman, M. M., "Damage Detection from Changes in Curvature Mode Shapes", *Journal of Sound and Vibration*, Vol. 145, No. 2, 1991, pp. 321~332
6. Chance, J., Tomlinson, G. R., and Worden, K., A Simplified Approach to the Numerical and Experimental Modeling of the Dynamics of a Cracked Beam, Proc. of the 12th Int. Modal Analysis Conference, Honolulu, Hawaii, Vol. 1, 1994, pp.778~785
7. Stubbs, N., and Osegueda, R., "Global Non-destructive Damage Evaluation in Solids", *Int J. Analytical and Experimental Modal Analysis*, Vol. 5, No. 2, 1990, pp.67~79
8. Wu, X., Ghaboussi, J., and Garrett, J. H., "Use of Neural Networks in Detection of Structural Damage", *Computers and Structures*, Vol. 42, No. 4, 1992, pp.649~659
9. Kaouk, M., and Zimmerman, D. C., "Structural Damage Assessment Using a Generalized Minimum Rank Perturbation Theory", *AIAA J.*, Vol. 32, No. 4, 1994, pp.836~842
10. Stubbs, N., Kim, J. T., and Topole, K., "The Effect of Model Uncertainty on the Accuracy of Global Nondestructive Damage Detection in Structures", Computational Stochastic Mechanics, eds. P.D. Spanos and C. A. Brebbia, Elsevier Applied Science, London, 1991, pp.125~136
11. Ostachowicz, W. M. and Krawczuk, M., "Vibration Analysis of a Cracked Beam", *Computers & Structures*, Vol. 36, No. 2, 1990, pp.245~250
12. Sundermeyer, J. N., and Weaver, R. L., "On Crack Identification and Characterization in a Beam by Nonlinear Vibration Analysis", TAM Report No. 74, UILU-ENG-93-604, Univ. of Illinois, 1993
13. Kim J. T., "Assessment of Relative Impact of Model Uncertainty on the Accuracy of Nondestructive Damage Detection in Structures", Ph.D. Dissertation, Texas A&M University, U.S.A., 1993
14. Chen, J., and Garba, J.A., "On-Orbit Damage Assessment for Large Space Structures", *AIAA Journal*, Vol. 26, No. 9, 1988, pp.1119~1126
15. Pandey A. K., and Biswas, M., "Damage Detection in Structures using Changes in Flexibility", *Journal of Sound and Vibration*, Vol. 169, 1994, pp.3~17
16. Stubbs N., and Kim, J. T., "Damage Localization in Structures Without Baseline Modal Parameters", *AIAA Journal*, Vol. 34, No. 8, 1996, pp.1649~1644

17. Farrar, C. R., and Jauregui, D. A., "Comparative Study of Damage Identification Algorithm Applied to a Bridge: I. Experiment", *Smart Mater. Struct.*, Vol. 7, 1998, pp.704~719
18. Kim, J. T., and Stubbs, N., "Improved Vibration-Based Damage Identification Method", Vol. 12, No. 3, 1999, pp.331~343
19. Kim, J. T., "Experimental Verification of Nondestructive Crack Detection Model Using a Few Natural Frequencies", *Journal of the Computational Structural Engineering Institute of Korea*, Vol. 12, No. 2, 1999, pp.149~159
20. Gudmunson, P., "Eigenfrequency Changes of Structures due to Cracks, Notches or Other Geometric Changes", *J. Mech. Phys. Solids*, Vol. 30, No. 5, 1982, pp.339~353
21. Kim, J. T., and Stubbs, N., "Model Uncertainty and Damage Detection Accuracy in Plate-Girder Bridges", *Journal of Structural Engineering*, ASCE, Vol. 121, No. 10, 1995, pp.1409~1417.
22. Saiidi, M., Douglas, B., and Feng, S., "Prestress Force Effect on Vibration Frequency of Concrete Bridges", *Journal of Structural Engineering*, ASCE, Vol. 120, No. 7, 1994, pp.2233~2241